

Microoptical Characterization and Modeling of Positioning Forces on *Drosophila* Embryos Self-Assembled in Two-Dimensional Arrays

Xiaojing Zhang, *Member, IEEE*, Chung-Chu Chen, *Member, IEEE*, Ralph W. Bernstein, *Member, IEEE*, Stefan Zappe, *Member, IEEE*, Matthew P. Scott, and Olav Solgaard, *Member, IEEE*

Abstract—In this paper, we describe high-precision experimental and numerical characterization of the positioning forces acting on *Drosophila* embryos that have self-assembled onto 2-D arrays of hydrophobic sites on a silicon substrate in water. The forces measured using a surface micromachined optical-encoder force sensor operating in reflection, are in good agreement with numerical simulations based on an extended surface energy model for the oil-based fluidic system. The positioning forces of ellipsoidal embryos on flat sites show a linear-spring-like relationship between the force and displacement on rectangular as well as cross-shaped sites. An average detachment force of $8.9 \mu\text{N} \pm 1.3 \mu\text{N}$ was found for the immobilized embryos on $250 \mu\text{m} \times 100 \mu\text{m}$ sites. The cross-shaped site has only 19.85% of the area of the rectangular site, but provides a comparable positioning force with a significant reduction in embryo clustering. In contrast, the positioning forces of flat silicon chips, similar in size to the embryos, are linear in the displacement only over a limited range ($0 \sim 40 \mu\text{m}$), and are then constant up to the detachment force ($25.0 \mu\text{N} \pm 3.5 \mu\text{N}$). Our measurements also show significant hysteresis in the force vs. displacement, indicating that variations in the surface properties play an important role in the self-assembly process. [1286]

Index Terms—Capillary force, *Drosophila* embryo, force sensor, optical encoder, self-assembly, surface energy, surface tension.

I. INTRODUCTION

FLUIDIC self-assembly [1]–[3] is an emerging microfabrication technology that simplifies production of a variety of hybrid structures, such as electrically functional three-dimen-

Manuscript received February 28, 2004; revised December 29, 2004. This work was funded by DARPA [Bio:Micro:Info] program (MDA972-00-1-0032). The device fabrication and characterization were performed at the National Nanofabrication Users Network (NNUN) facilities and Edward L. Ginzton Lab at Stanford University. Subject Editor D. J. Beebe.

X. Zhang is with the Department of Biomedical Engineering, and Microelectronics Research Center at J. J. Pickle Research Campus, The University of Texas at Austin, Austin, TX 78758, USA (e-mail: xjzhang@stanfordalumni.org).

C.-C. Chen was with Stanford University, Stanford, CA 94305 USA. He is now with Smart Sensors and Integrated Microsystems (SSIM), Wayne State University, Detroit, MI 48202 USA (e-mail: chungchu@ieee.org).

R. W. Bernstein is with SINTEF Electronics and Cybernetics, Department of Microsystems, NO-7465 Trondheim, Norway.

S. Zappe was with the Stanford Microphotonics Laboratory at Stanford University, CA 94305 USA. He is now with the Department of Biomedical Engineering, Carnegie Mellon University, Pittsburgh, PA 15213–3890 USA.

M. P. Scott is with Stanford University School of Medicine, Stanford, CA 94305 USA.

O. Solgaard is with Edward L. Ginzton Laboratory, and the Department of Electrical Engineering, Stanford University, CA 94305 USA.

Digital Object Identifier 10.1109/JMEMS.2005.851834

sional (3-D) networks generated by polyhedra patterned with solder dot and wires [4], [5], MEMS actuators with integrated dielectric mirrors that are positioned with submicron alignment precision [6], cylindrical displays fabricated by assembling light-emitting diodes onto flexible substrates [7], integrating optoelectronic devices on silicon VLSI for high-bandwidth communication applications [8], and high-Q, micron-sized helical and toroidal inductors [9]. Recently this technique has also been shown to enable immobilization and positioning of *Drosophila* (fruit fly) embryos in two-dimensional (2-D) arrays for parallel injection of genetic material [10]. High-throughput microinjection is essential for studying large numbers of genes and gene combinations in the *Drosophila* genome (13 600 genes [11]) through RNA interference (RNAi) [12], [13]. For automated genome-wide RNAi screens, arrays of embryos were self-assembled and aligned with matching arrays of microinjectors, facilitating injection of a large number of embryos in parallel [10]. During the self-assembly process, some degree of misalignment of the embryos is unavoidable. The force required to penetrate the immobilized embryos [14], as well as the embryo positioning force, are critical parameters that set the limits on the alignment accuracy required to achieve satisfactory injection yields. In this paper, we present experimental and numerical characterization of the positioning forces on *Drosophila* embryos in 2-D fluidic self-assembly arrays of various shapes. These results will facilitate our ultimate aim, which is the construction of automated systems for genome-wide RNAi screens of *Drosophila* embryos.

II. FLUIDIC SELF-ASSEMBLY

The applied *Drosophila* embryo immobilization method is based on fluidic assembly adopted from [6], with a modified assembly layer combination to make it suitable for biological samples [10]. Oxidized silicon substrates were first patterned with rectangular and cross-shaped Cr/Au ($100 \text{ \AA}/1000 \text{ \AA}$) sites. After immersing the substrates in a solution of 1 mM octadecanethiol in ethanol, hydrophobic sites were established by formation of self-assembled monolayers (SAMs) on the Au surfaces, while the silicon substrate was kept hydrophilic. The whole wafer was finally covered with a film of polychlorotrifluoro-ethylene based oil. The oil is known to be inert, have low toxicity, and regularly be used to cover *Drosophila* embryos

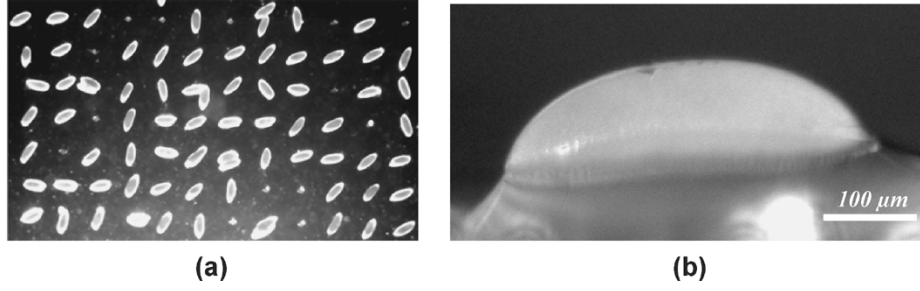


Fig. 1. (a) A 7×12 array of *Drosophila* embryos positioned on a fluidic self-assembly positioning chip. Immobilization gold site size: $250 \mu\text{m} \times 100 \mu\text{m}$, pitch: $1000 \mu\text{m} \times 1000 \mu\text{m}$. (b) Magnified view of a *Drosophila* embryo positioned and immobilized on the site through a thin film of polychlorotrifluoro-ethylene oil.

during injection experiments and hatching to prevent dehydration of the embryos. The wafer is then immersed in water. As a result, embryos were immobilized only at the oil-covered sites. Embryos that had not been immobilized were removed by a gentle rinse. Fig. 1 shows an array of embryos positioned on a SAM chip with a 7×12 array of rectangular gold sites with dimensions $100 \mu\text{m} \times 250 \mu\text{m}$ and a large pitch period of $1000 \mu\text{m} \times 1000 \mu\text{m}$ to reduce embryo clustering. For the fluidic self assembly arrays to achieve high alignment yield, the immobilization force and potential energy profile must be optimized.

III. MODELING AND SIMULATION OF FLUIDIC SELF-ASSEMBLY

We present a model and computational tools for efficient analysis and simulation of fluidic self-assembly of biological samples. A model will enhance the understanding of the underlying physics of the self-assembly process, while reliable simulation tools can significantly reduce the number of trial-and-error experimental reiterations required to optimize the binding site shape. Böhringer *et al.* [15] proposed a surface-energy model for self-assembly of flat silicon parts. However, this model is not applicable to the present study because it is based on the assumptions 1) that the micropart and binding site have the same hydrophobic coating, 2) that the adhesion oil layer between the self-assembled part and the binding site is negligible, and 3) that all surfaces are rigid and flat. We extend Böhringer's model to systems with different surface properties and ellipsoidal self-assembled parts. Fig. 2 shows the comparison of modeling for fluidic self-assembly of rigid, flat microparts and soft, curved *Drosophila* embryos. The difference in surface energy, ΔE , of the extended model can be represented by

$$\begin{aligned} \Delta E = & (\gamma_{\text{Embryo-H}_2\text{O}} - \gamma_{\text{Embryo-Oil}}) \\ & \cdot \Delta A_{\text{Embryo-H}_2\text{O}} + \gamma_{\text{Oil-H}_2\text{O}} \\ & \cdot \Delta A_{\text{Oil-H}_2\text{O}} + (\gamma_{\text{SAM-H}_2\text{O}} - \gamma_{\text{SAM-Oil}}) \\ & \cdot \Delta A_{\text{SAM-H}_2\text{O}} \end{aligned} \quad (1)$$

where γ_{x-y} is the surface tension between the media x and y . ΔA_{x-y} represents the area change on the interface of the media x and y during the assembly process. Initially, the SAM site is fully covered by oil, and the oil and the embryo are separated by water. After assembly, the embryo is in contact with oil, leading to a reduction of the areas that are in contact with water; thus $\Delta A_{\text{Embryo-H}_2\text{O}}$ and $\Delta A_{\text{Oil-H}_2\text{O}}$ are negative. Part of the oil

volume migrates from the edges of the site to the surface of embryo, and some parts of the sites may be exposed to water, i.e., $\Delta A_{\text{SAM-H}_2\text{O}}$ is positive. In thermodynamic equilibrium, the surface tensions are balanced at the contact line of water and oil on the solid surface [16]

$$\gamma_{\text{Solid-H}_2\text{O}} - \gamma_{\text{Solid-Oil}} - \gamma_{\text{H}_2\text{O-Oil}} \cos(\theta) = 0. \quad (2)$$

Therefore, the surface tension difference, $(\gamma_{\text{Embryo-H}_2\text{O}} - \gamma_{\text{Embryo-Oil}})$ and $(\gamma_{\text{SAM-H}_2\text{O}} - \gamma_{\text{SAM-Oil}})$, in (1) can be obtained by contact angle (θ) measurements, giving the surface tension, $\gamma_{\text{H}_2\text{O-Oil}} = 52 \text{ mJ/m}^2$ [6]. The measured average contact angle and calculated interfacial tension are shown in Table I. It is worth noting that the interfacial energies between hydrophobic surfaces and oil are relatively small, i.e., $\gamma_{\text{SAM-Oil}} \ll \gamma_{\text{SAM-H}_2\text{O}}$ and $\gamma_{\text{Embryo-Oil}} \ll \gamma_{\text{Embryo-H}_2\text{O}}$.

The three-interface system comprises a flat binding site, the ellipsoidal surface of the embryo and the meniscus of the oil, which is not in contact with the site or embryo. The edges of the oil meniscus are constrained to the hydrophobic binding site and embryo surface. The lower edges of oil are constrained on the binding site at $z = z_0$, as shown in Fig. 3. The complete assembly is immersed in water, so the water-site interface must be taken into account. Let A_{SAM} be the SAM site area, $A_{\text{SAM-Oil}}$ the area of the SAM-oil interface, and $A_{\text{SAM-H}_2\text{O}}$ the area of the SAM-water interface. The surface energy of the SAM site is

$$\begin{aligned} E_{\text{SAM}} = & \iint A_{\text{SAM-Oil}} \gamma_{\text{SAM-Oil}} dA \\ & + \iint A_{\text{SAM-H}_2\text{O}} \gamma_{\text{SAM-H}_2\text{O}} dA \\ = & \iint A_{\text{SAM-Oil}} \gamma_{\text{SAM-Oil}} dA \\ & + \iint (A_{\text{SAM}} - A_{\text{SAM-Oil}}) \gamma_{\text{SAM-H}_2\text{O}} dA \\ = & \iint A_{\text{SAM-Oil}} (\gamma_{\text{SAM-Oil}} - \gamma_{\text{SAM-H}_2\text{O}}) dA + c \end{aligned} \quad (3)$$

where c is a constant that can be ignored since we are only concerned with energy differences. By Stokes' theorem, the area integral in (3) can be transformed into an edge integral around the oil edge on the SAM site

$$E_{\text{SAM}} = \oint_{\text{Edge}} (\gamma_{\text{SAM-Oil}} - \gamma_{\text{SAM-H}_2\text{O}}) \vec{z} \cdot d\vec{s} \quad (4)$$

where $\gamma_{\text{SAM-Oil}} \ll \gamma_{\text{SAM-H}_2\text{O}}$, and can be neglected in (4).

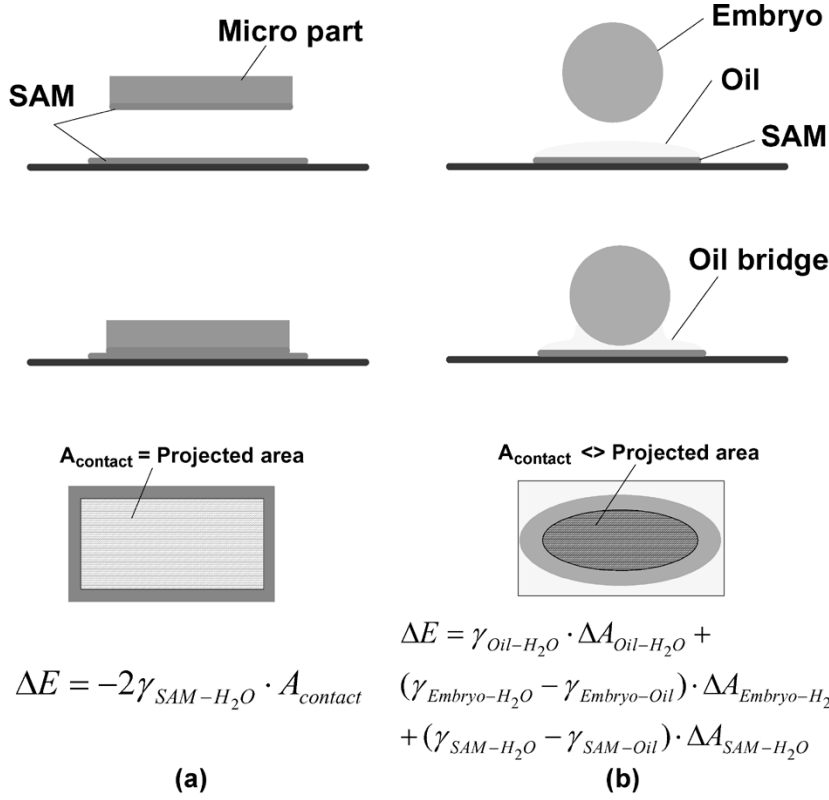

 Fig. 2. Comparison of fluidic self-assembly models for: (a) a flat micropart and (b) a curved biological samples, such as a *Drosophila* embryo.

 TABLE I
 AVERAGE CONTACT ANGLE AND INTERFACIAL ENERGY OF THE *DROSOPHILA* EMBRYO SELF-ASSEMBLY SYSTEM

<u>Interface</u>	<u>Contact Angle</u> (deg)	<u>Interfacial Tension</u> (mJ/m ²)
Oil – Water γ_{Oil-H_2O}	N.A.	52.2
SAM-Oil-Water $\gamma_{SAM-H_2O} - \gamma_{SAM-Oil}$	25	47.3
Embryo-Oil-Water $\gamma_{Embryo-H_2O} - \gamma_{Embryo-Oil}$	31	44.7

The upper faces of the oil, the interfacial area between the oil and the embryo, are constrained on the ellipsoidal wall of the embryo at $(x/R_1)^2 + (y/R_2)^2 + (z/R_3)^2 = 1$. The surface tension energy is calculated by direct integration over the embryo area covered by oil

$$E_{Emb} = \iint A_{Embryo-Oil} (\gamma_{Embryo-Oil} - \gamma_{Embryo-H_2O}) dA + c \quad (5)$$

where $\gamma_{Embryo-Oil}$ is much less than $\gamma_{Embryo-H_2O}$ and the constant c can be ignored.

The oil bridge (meniscus) consists of surface area exposed to water. This part of the surface may be moved freely without constraints. The surface tension energy of the oil bridge is also calculated by direct integration over the interfacial area between the oil and water

$$E_{BDG} = \iint A_{Oil-H_2O} \gamma_{Oil-H_2O} dA + c. \quad (6)$$

The restoring force applied on the embryo is the negative rate of change of total surface energy with respect to displacement of the rigid body. The principle of virtual work and the central finite difference method are employed to estimate the restoring force while the embryo is moved from its central stable position

$$F = -\frac{E(x + \Delta x) - E(x - \Delta x)}{2\Delta x} \quad (7)$$

The surface of oil is first evolved to an equilibrium state with minimum energy. A very small linear movement, Δx , is then applied to the embryo relative to the SAM pad in both positive and negative directions. The energy difference of $E(x + \Delta x)$ and $E(x - \Delta x)$ is of order Δx^2 , so it is not necessary to re-evolve the surface. Instead, the pressure is used to compensate for the slight volume change.

$$E(x + \Delta x) = E_{Surface}(x + \Delta x) - P(x) [V(x) - V(x + \Delta x)] \quad (8)$$

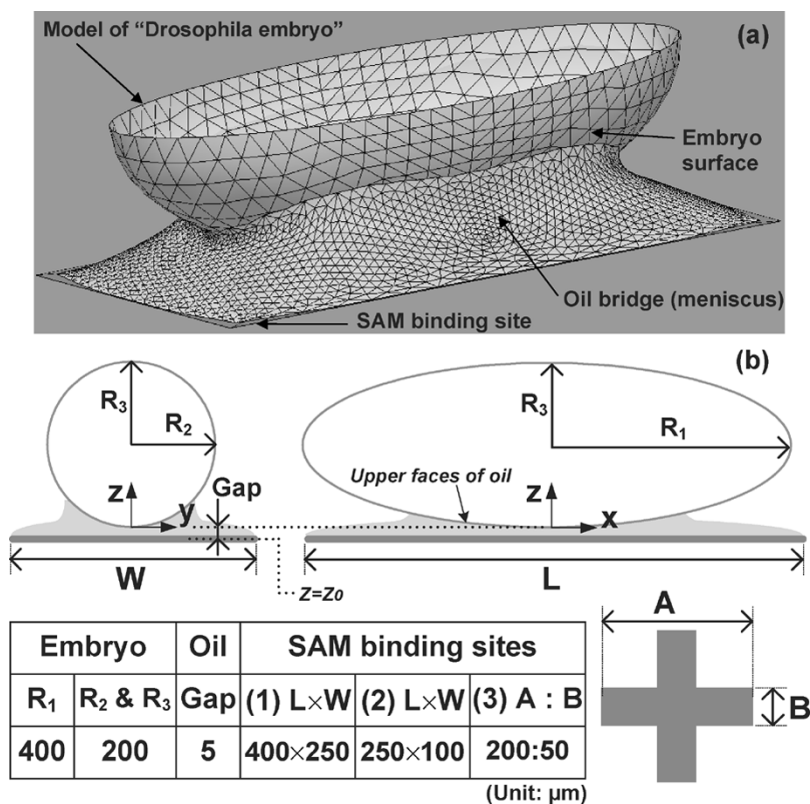


Fig. 3. (a) Simulated equilibrium shape of the oil bridge interfaces between Drosophila embryo and the $400 \mu\text{m} \times 250 \mu\text{m}$ SAM binding site. (b) Geometry and dimensions of the embryo and fluidic self-assembly site used in simulation and experiments.

where $E_{\text{Surface}}(x + \Delta x)$ is the surface energy recalculated after the displacement.

We programmed this model with (3)–(8) into Surface Evolver, a finite element software developed by Brakke [17]. An equilibrium shape of the interfaces was calculated, as shown in the example of Fig. 3(a) for embryo binding sites of $400 \mu\text{m} \times 250 \mu\text{m}$.

Fig. 3(b) shows the geometry and dimensions of the SAM site as well as an “ideal” Drosophila embryo. The ideal embryo has an ellipsoidal shape with the major axis, R_1 , of $400 \mu\text{m}$, and minor axes, R_2 and R_3 , of $200 \mu\text{m}$. Two rectangular ($400 \mu\text{m} \times 250 \mu\text{m}$ and $250 \mu\text{m} \times 100 \mu\text{m}$) and one cross site ($A = 200 \mu\text{m}$ and $B = 50 \mu\text{m}$) were investigated in the present study. Binding sites that are small compared to the embryo’s size were chosen to avoid multiple embryos on single sites. The oil gap is the distance between the bottom of the embryo and the site. This gap is difficult to measure precisely under the microscope, as indicated in Fig. 1(b). However, the simulation in Fig. 4 shows that both the positioning energy and force are weak functions of the oil gap within a $10 \mu\text{m}$ range.

IV. FORCE MEASUREMENTS

We reported earlier measurements of the adhesion force of embryos on bonding sites performed by observing the volumetric flow rate required for detaching the embryos [10]. This method yields measurement results with a large force variance ($\pm 60\%$ of the mean value). Here we use a more accurate measurement tool, which allows us to characterize the self-assembly

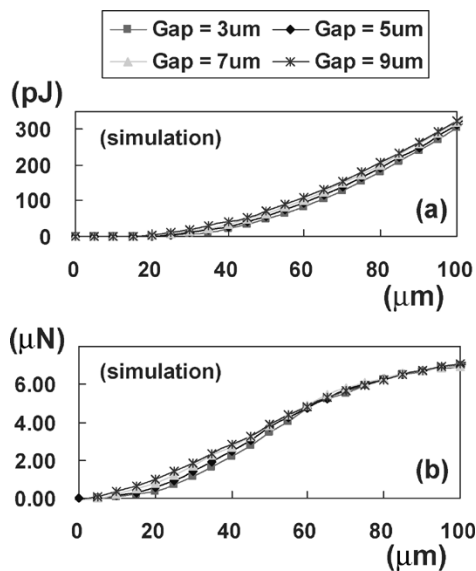


Fig. 4. Simulated positioning (a) energy and (b) force profiles of Drosophila embryos on SAM binding site with different oil gaps.

force and its displacement dependence in detail. The fabrication and calibration process of the encoder force sensor is presented in detail at [14]. Silicon nitride (Si_3N_4) is selected as the grating material due to the need for stress-optimized films of good optical quality. The optical transmission through the dual gratings was measured to be approximately 83% at the operating wavelength of 633 nm. The gratings therefore have only weak amplitude modulation, and the transmission encoder can be con-

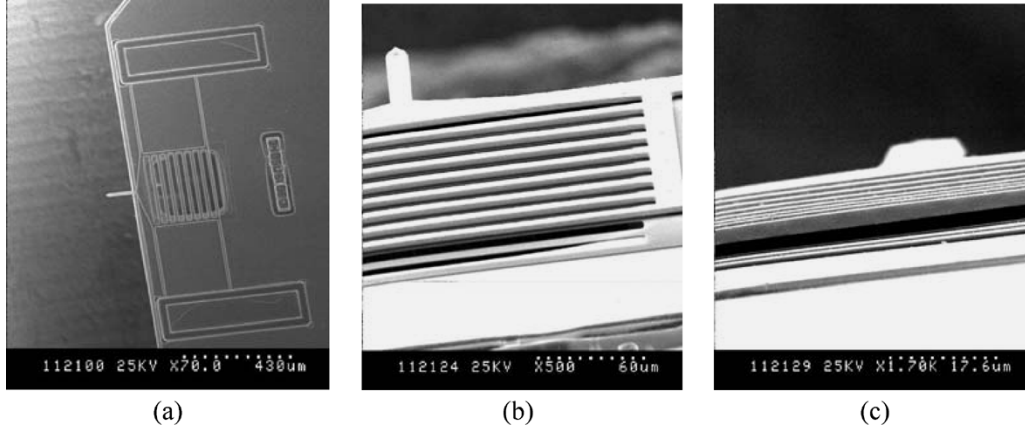


Fig. 5. SEM of (a) optical encoder force sensor integrated with the force probe. (b) Dual-grating sensing structure: the index grating on the top and the scale gratings underneath. Grating pitch is $20\ \mu\text{m}$ (c) magnified view of the vertical separation ($2\ \mu\text{m}$) between index grating and scale grating. Critical Point Drying (CPD) was performed to avoid unintended adhesion of the released index grating to the substrate.

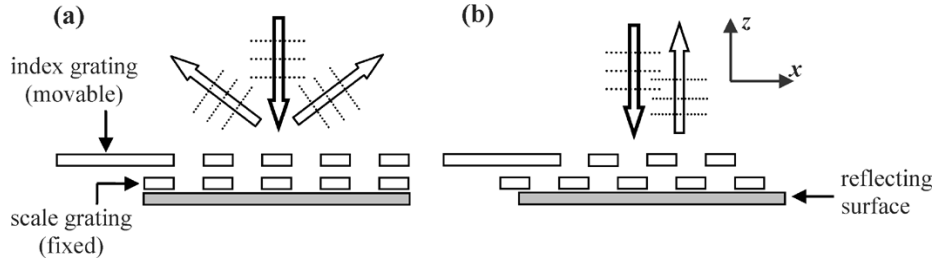


Fig. 6. Force measurement using MEMS optical encoder in reflection. The two extreme cases of (a) maximum diffraction and (b) maximum reflection are shown.

sidered to consist of pure phase gratings. Fig. 5 shows scanning electron micrographs (SEMs) of the integrated optical encoder force sensor with the force probe. Both gratings of the encoder had the pitch period of $20\ \mu\text{m}$, and their vertical separation was $2\ \mu\text{m}$. Critical Point Drying (CPD, the Automegasamdri-915B Critical Point tool, Tousimis, Rockville, MD)¹ was performed to avoid unintended adhesion of the released index grating to the substrate.

In earlier work on characterization of the microinjection forces penetrating *Drosophila* embryos [14], we used an integrated optical-encoder force sensor with configurable sensitivity and dynamic range. For the detachment force measurements, the encoder is operated in reflection as shown in Fig. 6. With no lateral force applied, the gratings of the encoder are aligned. When the probe applies a force to an embryo, the counter force displaces the index grating, which is attached to a mechanical spring of known stiffness. The displacement and therefore the positioning force are accurately determined by measurement of the diffracted light intensity. If $I_1(d)$ is the

intensity in the first diffraction order and d is the displacement of the probe, we have

$$I_1(d) = I_0 \cdot N^2 \cdot \left(\frac{\sin c^2 \left(\frac{N \cdot d}{2L} \right)}{\sin c^2 \left(\frac{d}{2L} \right)} \right) \cdot \left[(L - d) \cdot \sin c \left(\frac{L - d}{4L} \right) \right]^2 \cdot \sin^2(\phi_0) \cdot G(d) \quad (9)$$

$$G(d) = \begin{cases} \sin^2 \left[\frac{\pi \cdot (L + d)}{4L} \right] & d \in [0, L] \\ \sin^2 \left[\frac{\pi \cdot (3L - d)}{4L} \right] & d \in [L, 2L] \end{cases} \quad (10)$$

$$F = k_2 \cdot d \quad (11)$$

where N is the number of illuminated grating periods, $\phi_0(x)$ is the phase-delay for each grating element, $2L$ is the period of the grating with a 50% duty cycle, k_2 is the spring constant of the force sensor, and F is the embryo immobilization force.

The force measurement setup is shown in Fig. 7(a). The force sensor was illuminated by a HeNe laser with a spot size of $60\ \mu\text{m}$. The power of the first-order diffracted mode was measured with a photodiode placed 5 cm above the encoder. In the experiments, the encoder probes were aligned to be $100\ \mu\text{m}$ above the binding sites to ensure a fixed location of the acting point on the embryos. As shown in Fig. 7(b), the total stage displacement, x , is the sum of the bending of the nondehydrated embryo membrane, x_1 , the bending of the springs of the force sensor, x_2 , and the displacement of the embryo on the sites, x_3 . The membrane bending is relatively small due to the weak bonding force generated by the binding sites. Earlier results

¹Critical Point Drying (CPD) is used for carbon dioxide (CO₂) drying after release of bulk or surface micromachined devices. CPD is an efficient method of drying delicate samples without damaging its structure by surface tension that occurs when changing from the liquid to the gaseous phase. The release is usually performed by immersion of the device in hydrofluoric acid followed by subsequent immersions in several beakers of DI water. The CPD requires that the device be completely free of acid or water before introducing it to the chamber. To avoid this, the device should be placed in Isopropyl Alcohol for at least one hour.

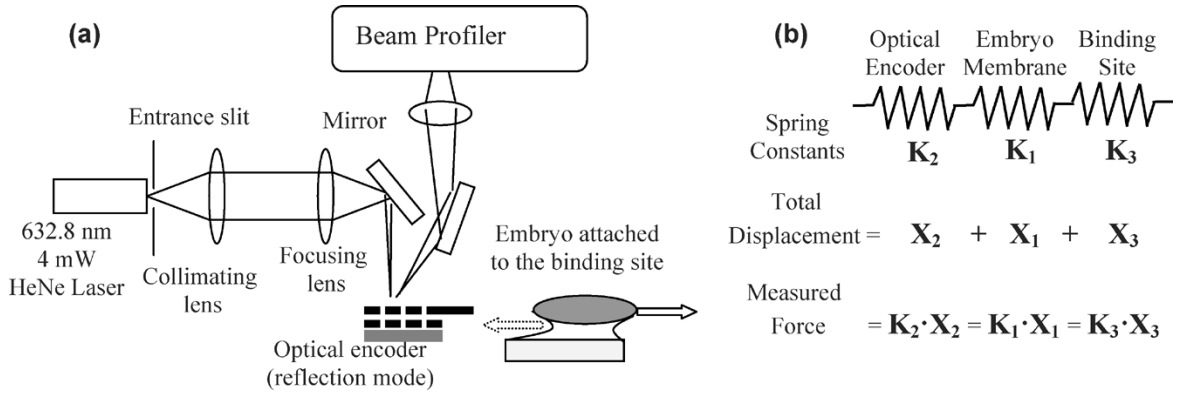


Fig. 7. (a) Positioning force measurement setup (not to scale). The optical force encoder has an $85 \mu\text{m}$ long probe, dual gratings with $20 \mu\text{m}$ pitch, $2 \mu\text{m}$ vertical separation, and a measured spring constant of $k_2 = 1.8 \text{ N/m}$. (b) A simplified spring model for the positioning force measurement system. The optical response of reflection-mode force sensor indicates the relative displacement, x_2 , between gratings.

show that the membrane deflection can be modeled as a linear spring with a spring constant $k_1 = 0.9 \text{ N/m}$, which means that the maximum membrane bending is less than $9 \mu\text{m}$ [14]. The membrane deformation can be regarded as small, and the equivalent spring constant of the assembly layer, k_3 , can be extracted. By properly designing the encoder spring constant, k_2 , the relative displacement, x_2 , of the two gratings can be determined by the periodic intensity variation in the diffraction orders. Therefore, the positioning force and the site potential energy as a function of embryo displacement can be estimated.

V. RESULTS

Fig. 8(a) shows the measured power of the first diffraction mode as a function of displacement of the stage for embryos positioned on $250 \mu\text{m} \times 100 \mu\text{m}$ rectangular sites. The encoder parameters are $N = 3$, $L = 10 \mu\text{m}$ and $k_2 = 1.8 \text{ N/m}$. The force sensor displacement can be calibrated from the known $20 \mu\text{m}$ period of the diffraction response. The significant deviation between the measurement and the calibration curve in Fig. 8(a) indicates the embryo detachment from the binding site. In a series of experiments, an average detachment force of $8.9 \mu\text{N} \pm 1.3 \mu\text{N}$ with 95% confidence intervals was found for the immobilized embryos. The interface between the binding site and embryo can be represented as an ideal spring with a spring constant k_3 of 0.07 N/m . This is in reasonable agreement with earlier controlled-fluidic detachment force measurements, but with much smaller variance ($\pm 14.1\%$ vs. $\pm 60\%$ of the mean). The measured force is integrated over the embryo displacement to get the quadratic potential energy profile (energy well depth 845 pJ), which is in good agreement with the simulated result, as shown in Fig. 8(b).

Self-assembly of flat silicon pieces has been studied by Srinivasan *et al.* [6] and Böhlinger *et al.* [15], but force measurements were not reported in either study. We fabricated rectangular $400 \mu\text{m} \times 250 \mu\text{m}$ test silicon pieces using a $300\text{-}\mu\text{m}$ -thick silicon substrate and evaporated 4 nm thin gold films (using a Hummer V Gold Sputter Coater, Refrac Systems, AZ) on one side. The pieces with one hydrophobic surface were pipetted onto a silicon substrate with matching SAM immobilization sites and were initially positioned with

minimum surface energy. Unbound parts were removed using flowing water. The differences between force vs. displacement of self-assembly of rigid, flat structures and curved biological samples are shown in Fig. 9. A constant restoring force of $25.0 \mu\text{N} \pm 3.5 \mu\text{N}$ was observed after an initial displacement of $44 \mu\text{m}$ and before detachment at $240 \mu\text{m}$. The initial linear rise of the force for the flat silicon pieces ($0 \sim 44 \mu\text{m}$) is similar to the spring-like behavior of the embryo positioning. The detachment force and displacement of the silicon pieces is about 2.5 times and 1.6 times, respectively, that of the embryo. Note that the binding site of the silicon piece is 4 times larger than that of the embryo's binding site. Our model is also capable of simulating the plateau-like as well as the sharp rising force profiles of the flat microparts, as shown in Fig. 9.

On cross-shaped binding sites, measurements were carried out with the force probe aligned along the two symmetry axes (x , y) of the embryos, as can be seen in Fig. 10. The simulated rising force profile fits well with the measurement up to detachment, but does not show the sharp falling edge after detachment. This is due to the nonbreaking oil layer assumption in the model. The measured small residual forces after embryo detachment are caused by the remaining oil trace being dragged over onto the hydrophilic substrate. The detachment force in the transversal direction (y) is about half that of the longitudinal direction (x). This indicates that embryo microinjection using cross-shaped binding sites should be performed at the embryo-end along the x direction. When the microinjectors are oriented off-normal by an angle β as shown in Fig. 11, the embryo will move until the restoring force from the adhesion layer is sufficiently large for penetration to take place. The embryo's movement, d_e , can be estimated assuming the embryo as a rigid body using

$$d_e = \tan(\beta) \frac{F_P}{k_3} \quad (12)$$

where F_P is the force required to penetrate the embryo, measured as $52.5 \mu\text{N} \pm 6.9 \mu\text{N}$ [14]. For large values of β , the embryos will be pushed off the binding site before penetration occurs. The critical values for x and y can be extracted from Fig. 10 at approximately $110 \mu\text{m}$ and $50 \mu\text{m}$ for the x and y directions, respectively. The corresponding critical angles for

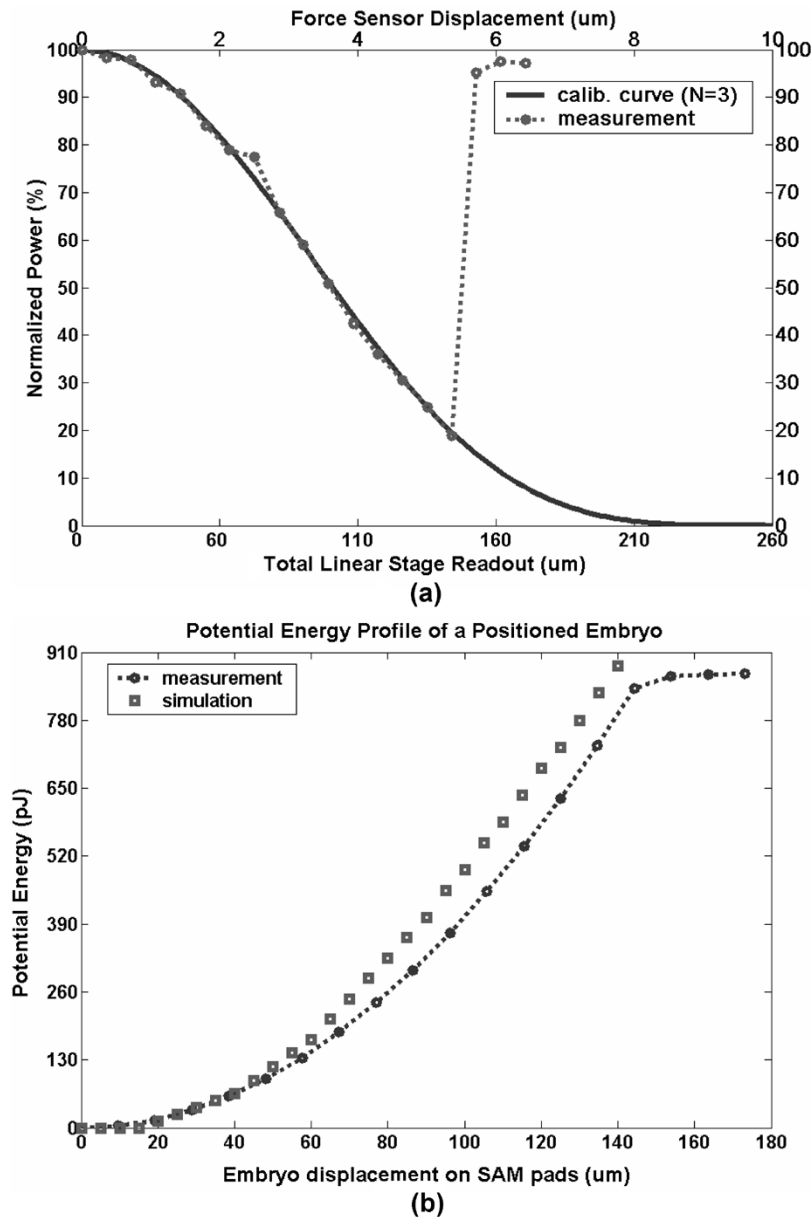


Fig. 8. Characterization of the positioning force on *Drosophila* embryos on $250 \mu\text{m} \times 100 \mu\text{m}$ binding sites using an optical encoder force sensor. (a) First diffraction mode power vs. probe displacement ($N = 3$, $L = 10 \mu\text{m}$, $k = 1.8 \text{ N/m}$). (b) The measured potential energy of an immobilized embryo is a quadratic function of displacement with an energy well depth of 845 pJ, in good agreement with the simulations.

off-normal incidence of the microinjectors are estimated at 9° and 4° , which indicate large angular tolerance for injectors aligned within the x - z plane. The cross-shaped binding site takes up only 19.85% of the area of the $250 \mu\text{m} \times 150 \mu\text{m}$ rectangular site, and has a smaller detachment displacement. However, it provides a comparable positioning force and reduces the chance of embryos being clustered on one binding site. Thus the cross-shaped binding site can be used for high-yield self-assembly within a compact chip area, while the rectangular-shaped sites can provide a larger self-positioning range for assembly under unexpected perturbations, for example from noisy working environment.

The special case of a rectangular binding site ($400 \mu\text{m} \times 250 \mu\text{m}$) shows the measured hysteresis effects along the long

direction of the immobilized embryos in Fig. 12(a) (circles). The suspected causes for hysteresis are chemical contamination, surface roughness and solutes in the liquid [16]. Since contamination usually causes a change of the surface properties, we added a single line defect of the interfacial tension in the simulation model at $x = -150 \mu\text{m}$ ($x = 0$ at site center) on the binding site. The higher interfacial tension on the defect line modified the shape of the nearby oil meniscus, as illustrated in the simulation inset in Fig. 12(b). Both the simulated and the measured force profiles in Fig. 12(a) clearly show the hysteresis and indicate a significant limitation on accuracy in the self-alignment process. The simulation predicted by a simple line defect shows different hysteresis characteristics from the measurements. To investigate the effect of the surface defect

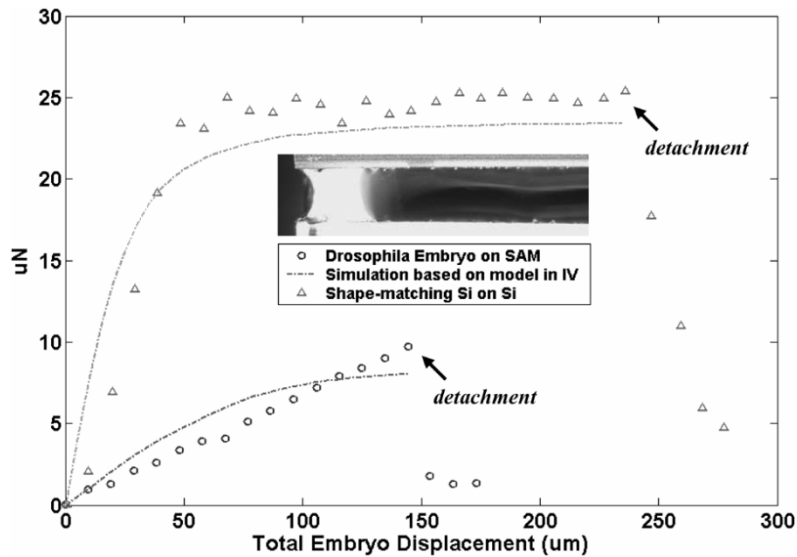


Fig. 9. Force measurement of fluidic self-assembly for a test silicon piece (thickness $300\ \mu\text{m}$) positioned on a $400\ \mu\text{m} \times 250\ \mu\text{m}$ binding site as shown on the embedded picture (data points in triangles). A constant restoring force of $25\ \mu\text{N}$ was observed during the majority (79%) of the movement. The force profile of the *Drosophila* embryo positioned on a $100\ \mu\text{m} \times 250\ \mu\text{m}$ binding site is shown by data points in circles. Simulated force profiles are plotted for comparison.

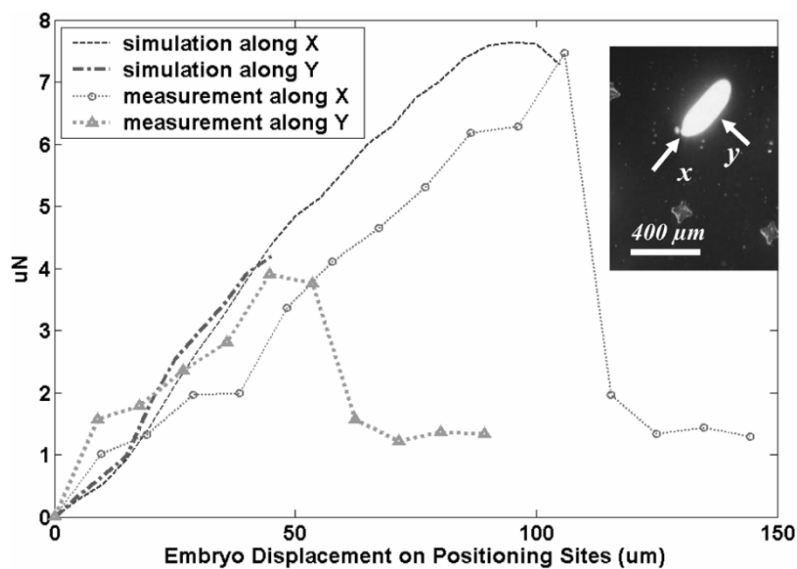


Fig. 10. Positioning force measurements along orthogonal directions on cross-shaped binding sites using encoder $N = 5$, $L = 10\ \mu\text{m}$, $k = 1.8\ \text{N/m}$. The adhesion force along the y direction is about half that of the x direction.

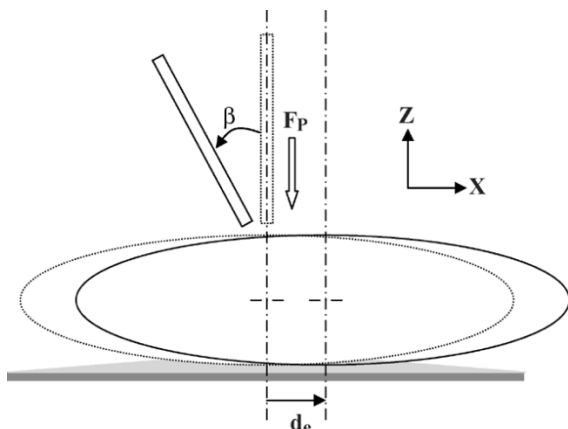


Fig. 11. Schematics showing the critical angle (β) for off-normal incidence of the microinjectors on *Drosophila* embryo self-assembled on positioning sites, where F_p is the force required to penetrate the embryo, d_e is the embryo's displacement in X -direction.

position on hysteresis, we changed the line defect position from $x = -150\ \mu\text{m}$ to $x = -50\ \mu\text{m}$ in the simulation and re-calculated the positioning forces, as shown in Fig. 13. As a line defect is placed closer to the center of the binding site, oil is more likely to cover the defect in order to reduce the area of oil exposed to water. As a result, the defect provides much less hysteresis for a small displacement [$0 \sim 40\ \mu\text{m}$ in Fig. 13(a)] of the embryo. However, if the defect occupies the edge, at a certain point of displacement the oil snaps through and leaves the whole defect line exposed to water. This causes larger hysteresis for larger embryo displacement, as shown in Fig. 13(b).

VI. CONCLUSION

Massive parallel self-assembly is emerging as an efficient and low-cost microfabrication technology for high throughput

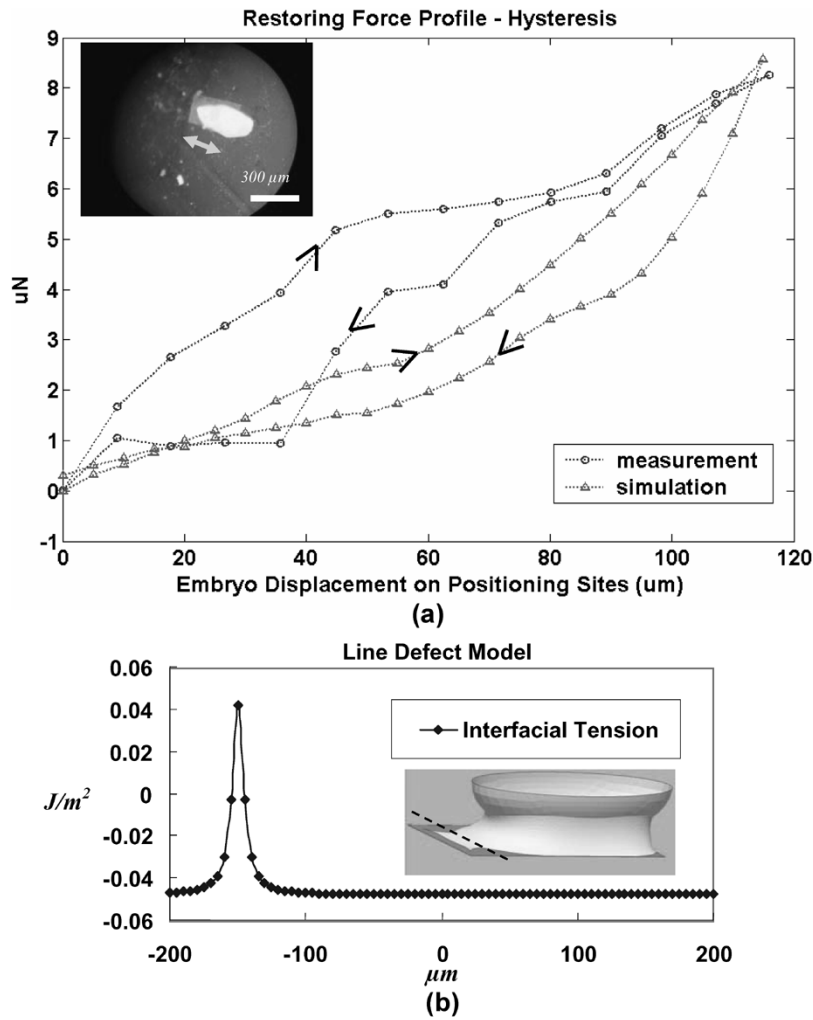


Fig. 12. Hysteresis of positioning forces of embryos on $400 \mu\text{m} \times 250 \mu\text{m}$ rectangular-shaped binding sites. (a) Shows measured and simulated restoring force profiles of immobilized embryos. (b) Shows the simple “line defect model” we use to simulate hysteresis.

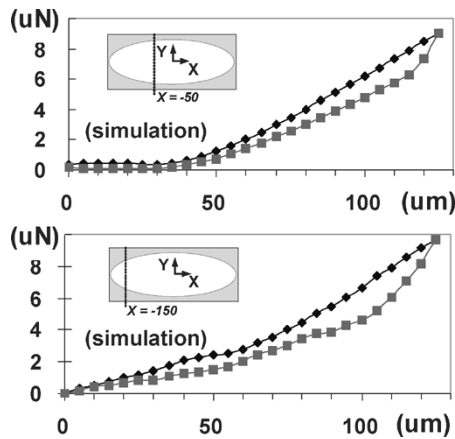


Fig. 13. Simulated effect of the line defect position on the hysteresis of embryo self-assembly positioning force: (a) line defect at $x = -50 \mu\text{m}$. As a line defect is closer to the center of the binding site, it is more favorable for the oil to cover the defect in order to reduce the area of the oil exposed to water. As a result, it provides much less hysteresis for a small displacement of the embryo. (b) Line defect at $x = -150 \mu\text{m}$. If the defect occupies the edge, at a certain point of displacement the oil snaps through and leaves the whole defect line exposed to water. This causes larger hysteresis for larger embryo displacement.

embryo and cell manipulation. In this paper we experimentally and numerically investigate self-assembly of *Drosophila* embryos onto 2-D arrays on a silicon substrate. A surface energy model of the self-assembly process of ellipsoidal samples is described and verified by high-precision force measurements using a micro-optical encoder, yielding results that potentially can be used for design optimization of fluidic self-assembly for a wide range of applications.

For *Drosophila* embryos self-assembled onto rectangular sites ($100 \mu\text{m} \times 250 \mu\text{m}$), a nearly linear relationship is found between the force and embryo displacement, with a spring constant of approximately 0.07 N/m . In comparison, flat silicon chips of dimensions similar to the embryos ($400 \mu\text{m} \times 250 \mu\text{m}$), have linear force vs. displacement characteristics only over a limited range and after that the force is constant up to detachment. For the ellipsoid-shaped embryos on cross-shaped sites, the detachment force in the longitudinal direction is twice that in the transversal direction. Compared to rectangular sites, the cross-shaped sites have a smaller maximum displacement before detachment while providing comparable positioning

force. Significant hysteresis is also found in the force vs. displacement, indicating that variation of surface properties may be a limitation on accuracy in the self-alignment process.

ACKNOWLEDGMENT

The authors would like to thank Prof. C. F. Quate and M. Fish for their collaboration and support.

REFERENCES

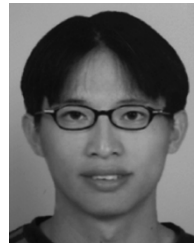
- [1] G. M. Whitesides and B. Crzybowski, "Self-assembly at all scales," *Science*, vol. 295, pp. 2418–2421, 2002.
- [2] M. B. Cohn, K. F. Böhringer, J. M. Noworolski, A. Singh, C. G. Keller, K. Y. Goldberg, and R. T. Howe, "Microassembly technologies for MEMS," in *Proc. SPIE Micromachining and Microfabrication*, 1998, pp. 2–16.
- [3] R. R. A. Syms, E. M. Yeatman, V. M. Bright, and G. M. Whitesides, "Surface tension self assembly of microstructures—the state of the art," *J. Microelectromech. Syst.*, vol. 12, no. 4, pp. 387–417, Aug. 2003.
- [4] D. H. Gracias, J. Tien, T. L. Breen, C. Hsu, and G. M. Whitesides, "Forming electrical networks in three dimensions by self-assembly," *Science*, vol. 289, pp. 1170–1172, 2000.
- [5] D. H. Gracias, M. Boncheva, C. Omeregic, and G. M. Whitesides, "Biomimetic self-assembly of helical electrical circuits using orthogonal capillary interactions," *Appl. Phys. Lett.*, vol. 80, pp. 2802–2804, 2002.
- [6] U. Srinivasan, D. Liepmann, and R. T. Howe, "Microstructure to substrate self-assembly using capillary forces," *J. Microelectromech. Syst.*, vol. 10, no. 1, pp. 17–24, Mar. 2001.
- [7] H. O. Jacobs, A. R. Tao, A. Schwartz, D. H. Gracias, and G. M. Whitesides, "Fabrication of a cylindrical display by patterned assembly," *Science*, vol. 296, pp. 323–325, 2002.
- [8] H. H. Yeh and J. S. Smith, "Fluidic self-assembly for the integration of GaAs light-emitting diodes on Si substrate," *IEEE Photon. Technol. Lett.*, vol. 6, pp. 706–708, 2004.
- [9] K. L. Scott, T. Hirano, H. Yang, H. Singh, R. T. Howe, and A. M. Niknejad, "High-performance inductors using capillary based fluidic self-assembly," *J. Microelectromech. Syst.*, vol. 13, no. 2, pp. 300–309, Apr. 2004.
- [10] R. W. Bernstein, X. J. Zhang, S. Zappe, M. Fish, M. Scott, and O. Solgaard, "Characterization of fluidic microassembly for immobilization and positioning of *Drosophila* embryos in 2-D arrays," *Sens. Actuators A: Phys.*, vol. 114, no. 2–3, pp. 191–196, 2004.
- [11] M. D. Adams *et al.*, "The genome sequence of *Drosophila melanogaster*," *Science*, vol. 287, March 24, 2000.
- [12] A. Schmid, B. Schindelholz, and K. Zinn, "Combinatorial RNAi: a method for evaluating the functions of gene functions in *Drosophila*," *Trends Neurosci.*, vol. 25, no. 2, pp. 71–74, 2002.
- [13] S. Zappe, M. Fish, M. P. Scott, and O. Solgaard, "Automated MEMS based fruit fly embryo injection system for genome-wide high-throughput RNAi screen," in *Proc. Int. Conf. on Micro Total Analysis System (μ TAS)*, Malmö, Sweden, Sep. 26–30, 2004, pp. 183–185.
- [14] X. J. Zhang, S. Zappe, R. W. Bernstein, O. Sahin, C.-C. Chen, M. Scott, and O. Solgaard, "Micromachined silicon force sensor based on diffractive optical encoders for characterization of microinjection," *Sens. Actuators A: Phys.*, vol. 114, no. 2–3, pp. 197–203, 2004.
- [15] K. Böhringer, U. Srinivasan, and R. T. Howe, "Modeling of capillary forces and binding sites for fluidic self-assembly," in *Proc. IEEE MEMS*, Interlaken, Switzerland, 2001, pp. 369–374.
- [16] P. G. de Gennes, "Wetting: statics and dynamics," *Rev. Modern Phys.*, vol. 57, no. 3, pp. 827–863, Jul. 1985.
- [17] K. A. Brakke, "The surface evolver," *Experimental Mathematics*, vol. 1, no. 2, pp. 141–165, 1992.



Xiaojing (John X. J.) Zhang (M'04) received the Ph.D. degree in electrical engineering from Stanford University, CA, in 2004.

His industrial experience includes working at Hewlett-Packard on the design of parallel optical interconnects, and at Cisco Systems on the design and evaluation of microphotonic devices and optoelectronic subsystems. From 2004 to 2005, he was a Research Scientist at Massachusetts Institute of Technology (MIT), Cambridge, and later, a Visiting Research Associate at the University of Chicago, IL.

In 2005, he joined the faculty at The University of Texas at Austin. Currently he is an Assistant Professor in the Department of Biomedical Engineering, and UT Microelectronics Research Center. His research interests are integration of photonics with microelectromechanical systems (MEMS) and microfluidic devices for *in vivo* imaging, biomanipulation, and nanoscale sensing. The actively pursued areas are microoptical imaging devices, miniaturized silicon instruments for microinjection and biomanipulation, fluidic self-assembly for microstructures and biological samples, ultrasonic microsurgical tools, and biological inspired MEMS (microelectromechanical systems) and nanotechnologies including sensor and actuator design, fabrication, and applications.



Chung-Chu Chen (M'03) received the B.Sc. degree in mechanical engineering from National Taiwan University, Taiwan, in 1994 and the Ph.D. degree in power mechanical engineering from National Tsing Hua University, Taiwan, in 1999.

He worked as an Engineer with Microsystem Technology Division, Electronics Research and Service Organization (ERSO) of the Industrial Technology Research Institute (ITRI), Taiwan, between 2000 and 2002. He held a Postdoctoral position in Stanford University and was conducting his research

at E.L. Ginzton Lab. He is currently a Research Fellow in Smart Sensors and Integrated Microsystems (SSIM) Program, Wayne State University. His research focuses on microfluidic device design, simulation, fabrication and characterization for several applications including cell manipulating and culturing, DNA analyzing, fluidic self-assembling, microdroplet injecting, and device cooling and he holds nine related patents.



Ralph W. Bernstein (M'04) received the Doctoral degree in physical electronics in 1990 from the Norwegian Institute of Technology (NTH), Trondheim, Norway.

He is now Research Director at SINTEF Electronics and Cybernetics, Department of Microsystems. He started at SINTEF as a Senior Scientist from 1992 and became Research Director in 1996. Previously, he was employed as a Research Scientist at Norwegian Telecom Research from 1990 to 1992.

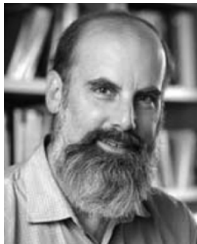
He was Associate Professor II at the University of Tromsø from 1996 to 2001. Bernstein was on leave from SINTEF as a Visiting Scholar at Ginzton Laboratory, Stanford University, CA, in 2001–2002. His fields of expertise are within III–V semiconductor technology, microsystem technology (MST), and MEMS design. His recent research interests have focused on BioMEMS for high throughput injection of biological material into embryos and cells.

Dr. Bernstein is a Member of the Technical Committee for the European EUREKA-program, EURIMUS, and is an evaluator within the thematic area IST of the 6th EU framework program.



Stefan Zappe (M'02) received the Diploma degree in electrical engineering from the Berlin University of Technology, Germany, in 1996. From 1996 to 2001, he worked as a Ph.D. student at the Microsensor and Actuator Center at the Berlin University of Technology.

In February 2001, he joined the Stanford Microphotonics Laboratory at Stanford University, CA, as a Postdoctoral Researcher. His research activities include microfluidic systems for cell- and embryo-handling, sorting and micro-injection; biology of fruit fly development; gene silencing by means of RNAi (RNA interference); microorifices for DNA shearing; microfluidic systems based reusable arrays for DNA sequencing; integration of active and passive optical components into microsystems.



Matthew P. Scott received the B.S. and Ph.D. degrees in biology from the Massachusetts Institute of Technology (MIT), Cambridge.

He did postdoctoral research at Indiana University and then joined the faculty at the University of Colorado at Boulder. In 1983, he moved to Stanford University School of Medicine, where he is now Professor of Developmental Biology and of Genetics. He has published more than 130 papers and three patents. His research areas are developmental genetics and cancer research, particularly the roles of signaling systems and transcriptional regulation in embryonic development. His research employs genetics, genomics, cell biology, and molecular biology in exploring how cells acquire their fates and are patterned. He is an editor of *Current Opinion in Genetics and Development* and of the *Proceedings of the National Academy of Sciences*. He is a past president of the Society for Developmental Biology, a member of the American Academy of Arts and Sciences, and a member of the National Academy of Sciences. He is presently chairing Stanford's Bio-X program, which is designed to accelerate the coming together of engineering, physics, and chemistry with biology and medicine.



Olav Solgaard (S'88-M'90) received the B.S. degree in electrical engineering from the Norwegian Institute of Technology and the M.S. and Ph.D. degrees in electrical engineering from Stanford University, CA.

He held a Postdoctoral position at the University of California at Berkeley, and an Assistant Professorship at the University of California at Davis, before joining the faculty of the Department of Electrical Engineering at Stanford University in 1999. His research interests are optical communication and measurements with an emphasis on semiconductor fabrication and MEMS technology applied to optical devices and systems. He has authored more than 150 technical publications, and holds 18 patents. He is a co-founder of Silicon Light Machines, Sunnyvale, CA, and an active consultant in the MEMS industry.